Identification of a Large Number of Spin-Wave Eigenmodes Excited by Parametric Pumping in Yttrium Iron Garnet Microdisks

T. Srivastava[1,*] H. Merbouche[2,†] I. Ngouagnia Yemeli,[1] N. Beaulieu,[3] J. Ben Youssef,[3]
M. Muñoz,[4] P. Che,[5] P. Bortolotti,[5] V. Cros,[5] O. Klein,[6] S. Sangiao,[7] J.M. De Teresa,[7]
S.O. Demokritov,[2] V.E. Demidov,[2] A. Anane,[5] C. Serpico,[8] M. d'Aquino,[8] and
G. de Loubens[1,‡]

[1]*SPEC, CEA, CNRS, Université Paris-Saclay, Gif-sur-Yvette, France*
[2]*Institute for Applied Physics, University of Muenster, Germany*
[3]*LabSTICC, CNRS, Université de Bretagne Occidentale, Brest, France*
[4]*Instituto de Tecnologías Físicas y de la Información (CSIC), Madrid, Spain*
[5]*Unité Mixte de Physique, CNRS, Thales, Université Paris-Saclay, Palaiseau, France*
[6]*Université Grenoble Alpes, CEA, CNRS, Grenoble INP, Spintec, Grenoble, France*
[7]*Instituto de Nanociencia y Materiales de Aragón (INMA) and Laboratorio de Microscopías Avanzadas (LMA),
Universidad de Zaragoza, Zaragoza, Spain*
[8]*Department of Electrical Engineering and ICT, University of Naples Federico II, Italy*

We present the parametric excitation of spin-wave modes in yttrium iron garnet (YIG) microdisks via parallel pumping. Their spectroscopy is performed using magnetic resonance force microscopy (MRFM), while their spatial profiles are determined by microfocus Brillouin light scattering (BLS). We observe that almost all the fundamental eigenmodes of an in-plane magnetized YIG microdisk, calculated using a micromagnetic eigenmode solver, can be excited using the parallel pumping scheme, as opposed to the transverse one. A comparison between the MRFM and BLS data on the one hand, and the simulations on the other hand, provides the complete spectroscopic labeling of over 40 parametrically excited modes. Our findings could be promising for spin-wave-based computation schemes, in which the amplitudes of a large number of spin-wave modes have to be controlled.

I. INTRODUCTION

Novel proposals for spin-wave (SW)-based computing schemes like reservoir and neuromorphic necessitate generating and controlling multiple SW modes [1–5]. The most standard way to excite SW modes in a magnetic microstructure is by direct inductive coupling. There, the quasiuniform microwave field, produced on the magnetic volume by an rf antenna, couples to the transverse dynamical component of the magnetization associated with the SW mode, with a maximal efficiency when the applied rf frequency coincides with the eigenfrequency of the mode. However, this method is not adapted to excite modes with antisymmetric spatial profiles, as their overlap integral with the excitation field is zero [6], nor short-wavelength modes, as their excitation efficiency quickly decreases with their wave vector. Yet, these two categories of modes make up a significant part of the SW k-space. In order to excite a large number of modes irrespective of their spatial profiles, parametric parallel pumping, which does not suffer from these limitations, becomes the ideal choice [7]. In this case, the microwave magnetic field created by the rf antenna is aligned parallel to the static field. As a result, it does not couple to the SW modes directly. Instead, it interacts with the dynamic component of magnetization oscillating at 2ω in the static field direction, which arises due to the elliptical trajectory of magnetization precession at ω. An rf field at 2ω can therefore excite SW modes at ω. A quantum mechanical picture of this process is a photon generating two magnons of opposite momenta at half its frequency [8]. Since this is a nonlinear process, SWs are excited only if the amplitude of the excitation field exceeds a parametric threshold, which depends on the mode relaxation and on the mode ellipticity. The threshold power is lower for lower relaxation rates and higher ellipticities.

Parallel pumping has been employed to generate SW modes in extended films [9–13] and micro- and nanowaveguides [14,15] of yttrium iron garnet (YIG), as well as in magnetic nanocontacts [16], magnetic tunnel junctions [17], and micro- and nanodots of Permalloy

---

*titiksha.srivastava@cea.fr
†hugo.merbouche@uni-muenster.de
‡gregoire.deloubens@cea.fr

[18–20]. It has also been used for SW amplification [21]. However, these studies have been limited to a handful number of modes. The excitation and identification of many modes in an adequate system would pave the way towards simultaneous control and manipulation of a large number of SW modes for different applications in magnonics. In particular, proposed spin-wave-based computing schemes like reservoir and neuromorphic could hence take advantage of the massive parallelization of operations in frequency space and of the nonlinear SW interactions.

In this study, we present the excitation and identification of multiple SW modes in YIG microdisks via parametric pumping. The scheme of the experiments is shown in Fig. 1. The SW modes are excited in YIG disks of diameters of 1, 3, and 5 µm through an integrated rf antenna and detected using a magnetic resonance force microscope (MRFM). Their spatial profiles can also be recorded using microfocus Brillouin light scattering (µ-BLS) spectroscopy. We observe that almost all the SW eigenmodes are accessible by parametric pumping. As expected, these eigenmodes become fewer in number as the size of the disk decreases. For the 3-µm disk, we label over 40 eigenmodes by comparing its MRFM parametric spectroscopy to micromagnetic simulations, and confirm the identification of as many as 10 of them through their profiles thanks to µ-BLS. Our results could be instrumental in designing basic units for unconventional computing schemes like neuromorphic computing using hyperconnected populations of many eigenexcitations in a single microstructure.
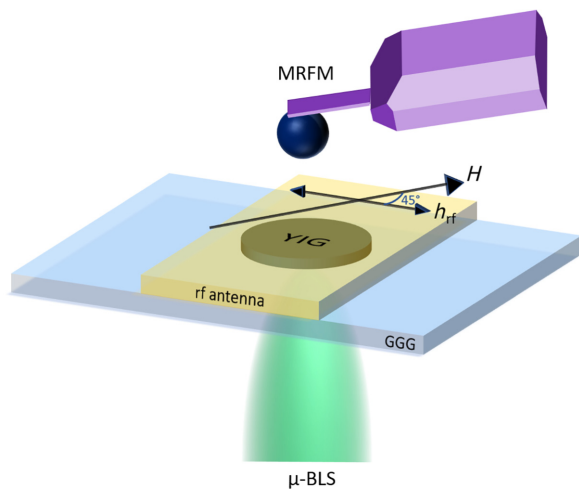

FIG. 1. Parallel pumping of a YIG microdisk using an rf antenna deposited on top. Spectroscopy of the parametrically excited modes is achieved using an MRFM positioned above the sample. Their spatial profiles are measured by µ-BLS using a separate experimental setup, the laser beam being focused to the bottom of the sample, through the transparent GGG substrate.

II. RESULTS

A. Sample

We use 50-nm-thick YIG grown on 0.5-mm-thick Gadolinium Gallium garnet $(Gd_3Ga_5O_{12})$ (GGG) substrate by liquid-phase epitaxy [22]. The characteristics of the extended film are measured by standard magnetometry and broadband ferromagnetic resonance (FMR) techniques. These yield a saturation magnetization $M_s = 140.7$ kA/m, a gyromagnetic ratio $\gamma = 28.28$ GHz/T, a Gilbert damping parameter $\alpha = 7.5 \times 10^{-5}$, and a weak inhomogeneous broadening of the FMR linewidth, found to be 0.1 mT. These parameters are typical of the YIG material; the exchange constant, which has not been specifically determined on this film, is assumed to be $A = 3.7$ pJ/m, a standard value from the literature [23]. The YIG layer is patterned into disks of diameters of 1, 3, and 5 µm using e-beam lithography. A 220-nm-thick Ti/Au antenna, of width equal to 8 µm, is then deposited on top of the disks. Injecting an rf current in the antenna generates an rf in-plane magnetic field that is orthogonal to the long axis of the antenna.

B. Parallel pumping spectroscopy

The SW mode spectroscopy is done using an MRFM. It employs a very soft cantilever, at the end of which a submicronic magnetic spherical probe made of cobalt is attached [24], to mechanically detect the magnetization dynamics in the sample placed underneath [25]. When SWs are excited in the sample by the microwave field, the (static) longitudinal component of magnetization is reduced and so is the dipolar force on the MRFM probe, resulting in a displacement of the cantilever beam, which is detected optically. The rf excitation applied to the sample via the antenna is modulated at the mechanical resonance frequency of the cantilever to improve the quality factor and the signal-to-noise ratio.

In these measurements, the dc magnetic field is applied in plane at an angle of 45° with respect to the direction of the rf magnetic field, as displayed in Fig. 1. Therefore the rf field excitation has both a transverse and a parallel component relative to the magnetization direction, which enables us to perform both direct and parametric excitation. The parallel pumped SW spectrum is studied for different-sized disks as a function of the microwave power at the rf generator output. Figure 2 shows the results of MRFM parametric spectroscopy performed at a constant microwave frequency of 4 GHz for the three disks (color-coded intensity maps), together with the corresponding transverse excitation spectra measured at a fixed frequency of 2 GHz and power of −5 dBm (continuous white curves). Only a few SW modes are detected in the latter regime. In contrast, we observe that a large number of modes can be excited by parallel pumping at 4 GHz for all the disks, in the range of applied dc field corresponding to the direct
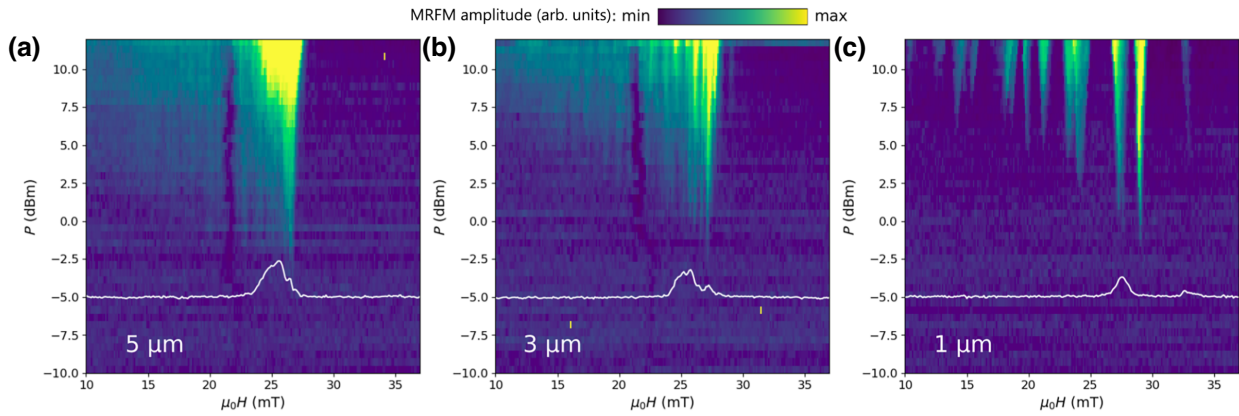
FIG. 2. Intensity maps of parametrically excited modes in the field-power coordinate excited by a microwave field of frequency 4 GHz, measured by MRFM on YIG disks of 5 µm (a), 3 µm (b), and 1 µm (c) in diameter. In each panel, the continuous white curve corresponds to the direct excitation spectrum at a frequency of 2 GHz. The rf pumping field h_{rf} is at 45° from the dc field H.

excitation of modes at 2 GHz, because parametrically excited modes are generated at half the pumping frequency. As expected, this occurs only above a minimum power level, which ranges from about −4 dBm for the 5-µm disk to −2 dBm for the 1-µm disk. The fact that the parametric threshold increases and that the density of the excited modes decreases as the lateral size decreases can be explained by geometrical confinement effects, as reported earlier [20].

In the following, we mainly focus on the 3-µm disk where the SW modes are quite abundant but at the same time discernible (not too closely spaced). We perform similar measurements on this disk, this time fixing the value of the dc field to 27 mT, and scanning the parallel pumping frequency as a function of the microwave power. Figure 3 shows the intensity map of the parametrically excited modes in these conditions, as a function of half the pumping frequency $f_p/2$ and rf power P, varied along the horizontal and vertical axes, respectively. We note that the threshold power increases with the frequency in a nonmonotonic way, which can be explained as follows. The threshold excitation field of each mode can indeed be computed as the ratio between the relaxation rate $\omega_r(k)$ and a coupling coefficient $V(k)$, which is related to the mode ellipticity [7]: the more elliptical a mode is, the larger its $V(k)$ and the lower will be its threshold. Both the terms depend nonmonotonically on the wave vector k and on the mode frequency. However, on a wide range, when k increases, so does the mode frequency and its relaxation rate, while its ellipticity and its coupling $V(k)$ tend to decrease [7,21]. This leads to the clear but not monotonic increase of the experimental threshold power with frequency seen in Fig. 3.

C. Simulations

In order to identify these parametrically excited modes, micromagnetic simulations using the eigenmode solver

implemented in the micromagnetic code MaGICo [26] are performed to calculate the SW spectrum. The magnetic ground state is first computed for the specific geometry and applied magnetic field. Once the magnetic ground state is known, the equation describing magnetization dynamics, the Landau-Lifshitz-Gilbert equation, is linearized around the ground state and small-amplitude spatial profiles of the modes are computed. This problem can be formulated as a generalized eigenvalue problem as described in Ref. [27]. The solution of the eigenvalue problem allows the determination of the SW spectrum of the magnetic sample under
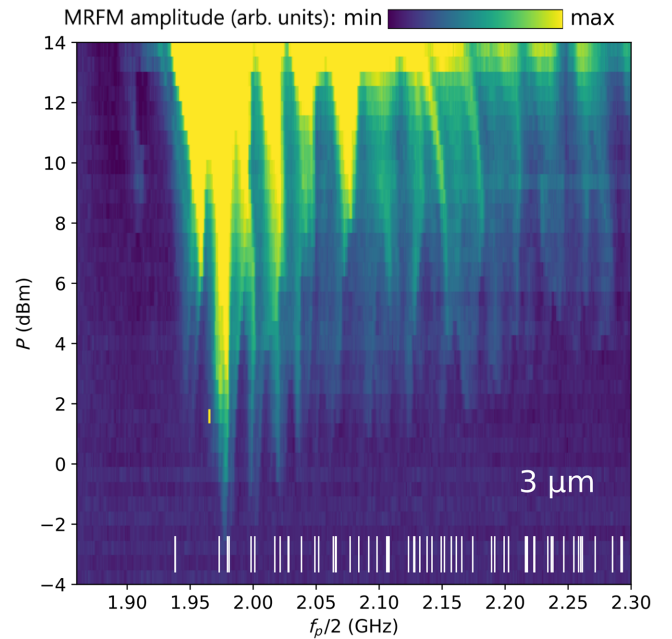

FIG. 3. Comparison between parametric spectroscopy MRFM data (color-coded intensity map) and computed eigenfrequencies (white vertical ticks) of the 3-µm disk. The in-plane dc field is set to 27 mT.

investigation. Here, the geometry of the body, a 50-nm-thick disk of 3 μm in diameter, is discretized using $300 \times 300 \times 5$ cubic cells (mesh size of $10 \times 10 \times 10$ nm^3), and the values of the magnetic parameters used in the simulation are those determined experimentally. As in the experimental case, the applied field lies in the plane of the disk and is set to 27 mT. The implementation of suitable matrix-free large-scale methods described in Ref. [28] allows the calculation of hundreds of eigenmodes for such an extended structure (353 440 computational cells, eigenvalue problem size 706 880 $\times$ 706 880) in a few hours.

Figure 4 displays the computed spatial profiles of the 11th to 31st lowest frequency eigenmodes, ordered by their frequency. The 10 lowest frequency modes, not shown in the figure, lie between 0.84 and 1.85 GHz and correspond to edge modes, where the precession of the magnetization is strongly confined at the boundaries of the disk, in the horizontal direction of the applied dc field due to the demagnetizing field [29,30]. The following modes correspond to standing SW modes, which can be labeled by the number of precession lobes in the horizontal (n_x) and vertical (n_y) directions. For instance, mode 20 (second row, third column) can be labeled by $n_x = 2$ and $n_y = 1$, i.e., it is the (2,1) mode. Mode 24 (second row, last column) is the (5,2) mode. The most uniform mode, usually referred to as the FMR mode, is mode 29 (third row, fifth column), or mode (1,1).

Figure 3 presents a comparison between the experimental spectroscopy and the computed eigenfrequencies of

modes 11 to 69 (see Fig. 6 in the Appendix for a visualization of the 100 lowest frequency modes), shown as white ticks on top of the intensity map of the parametrically excited modes. We observe a good agreement between the computed mode frequencies and the experimental mode frequencies (at half-pumping frequencies $f_p/2$) observed at the bottom of the parametric instability regions (elongated yellow-green triangles extending downwards on the intensity map). From this comparison, it is possible to state that almost all, if not all, SW eigenmodes can be parametrically excited, irrespective of their spatial profile. Due to the high density of modes in the investigated frequency range, we only focus on a few modes, to emphasize the good agreement noted above. The lowest lying computed modes in Fig. 3 are the pair of modes 11 and 12 with respective frequencies of 1.938 and 1.9383 GHz, which correspond rather well to the measured parametric instability region with a threshold power of 2 dBm at around 1.95 GHz. The small disagreement of 10 MHz between the computed and measured frequencies is not unexpected, since these modes belong to the category of edge modes, whose characteristics are very sensitive to imperfections at the periphery of the disk [30,31], which are not taken into account in the simulations. If we move to the next parametrically excited modes, which have the lowest power threshold and have frequencies around 1.975 GHz, the comparison with computed frequencies shows that they correspond to two pairs of modes: modes 13 and 14 with respective frequencies 1.973 and 1.9731 GHz and modes 15 and 16 at 1.9796
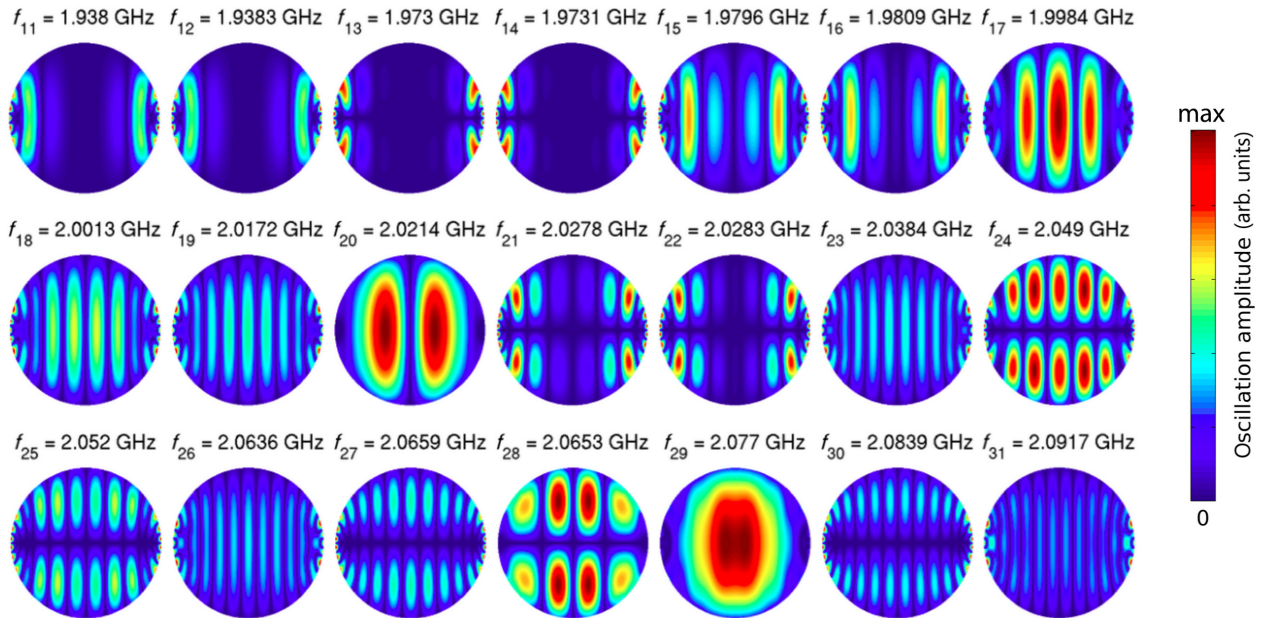

FIG. 4.   Computed spatial profiles of the 11th to 31st lowest frequency modes of the 3-μm-diameter YIG disk, in-plane magnetized by a field of 27 mT applied along the horizontal direction. The color code refers to the oscillation amplitude (absolute value) of the local magnetization. Adjacent precession lobes are in opposite phase to each other for most modes.
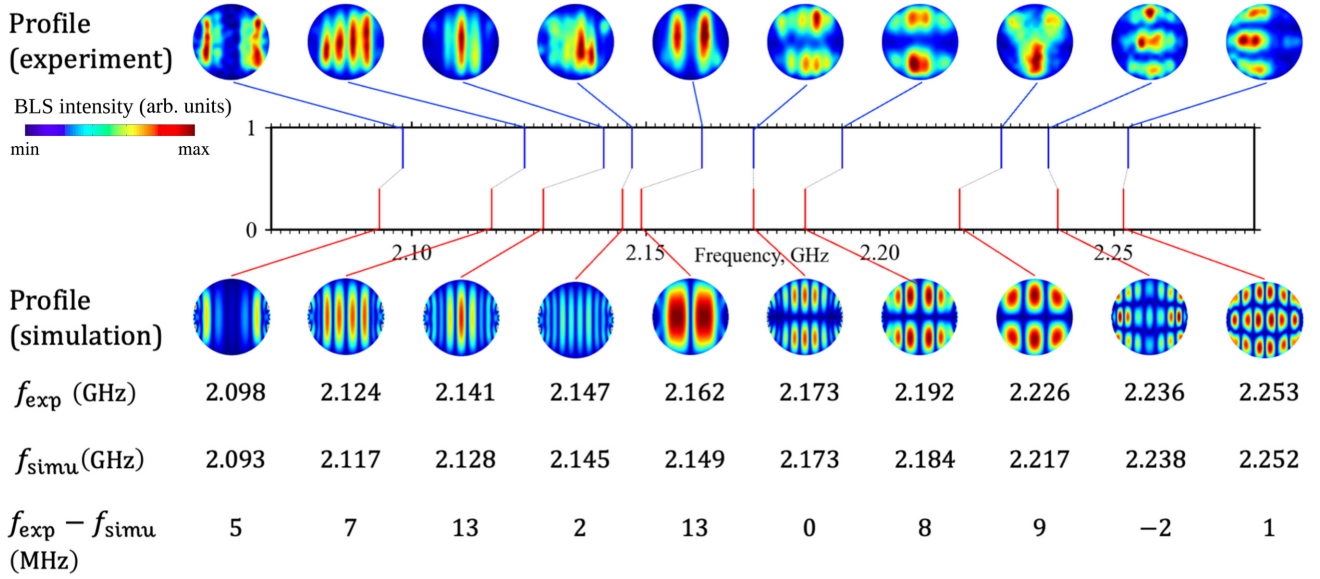
FIG. 5. The central graph displays the BLS-detected frequencies at 30 mT for 10 modes of the 3-μm disk (blue lines) and the corresponding computed frequencies of eigenmodes (red lines). These frequencies are matched (dotted dark lines) by associating the mode profiles measured by BLS imaging (above the graph) with those computed in the simulation (below). The experimental and simulated mode frequencies (in GHz) and their differences (in MHz) are given in the table.

and 1.9809 GHz. The next excited modes in the experimental spectroscopy map are at around 2 GHz, and they correspond to mode 17 at 1.998 GHz and mode 18 at 2.001 GHz. As a matter of fact, a detailed inspection of the data shows that, indeed, the parametric instability region has two nearby minima with frequencies equally spaced around 2 GHz. This good agreement between experimental and computed mode frequencies continues over the full range of investigated frequencies. We note that among the 59 modes whose frequencies are shown as white ticks in Fig. 3, only 44 modes have discernible frequencies and spatial profiles, a few of them being pairs of modes with very similar characteristics (e.g., pairs of modes 11 and 12, 13 and 14, 15 and 16, 21 and 22, etc.).

D. Spatial profiles with μ-BLS

To push further the comparison between computed SW modes and experiments, it is possible to take advantage of μ-BLS, to map the spatial profiles of dynamic magnetization in microstructures [32]. A probing laser light ($\lambda = 473$ nm and $P_{laser} = 0.1$ mW) is focused into a diffraction-limited spot on the surface of a similar 3-μm YIG disk (Fig. 1) and the modulation of this probing light by the magnetization oscillations is analyzed using a high-contrast optical spectrometer. The obtained signal—the BLS intensity—is proportional to the intensity of the magnetic oscillations at a given frequency. In this BLS measurement, the in-plane bias field is set at 30 mT. To compare the experimental mode profiles with the computed mode profiles, the micromagnetic simulations are

therefore repeated at 30 mT as well. To determine the mode frequencies, the pump frequency f_p is scanned with a 2-MHz step and the BLS intensity at $f_p/2$ is recorded at a certain point of the disk, chosen to be off-centered by 0.5 μm in both x and y directions to favor the detection of even and high-order modes. We pick a dozen different mode frequencies and image the corresponding profiles by sweeping the laser spot position across the disk with an 0.2-μm step (17×17 points). Figure 5 presents the comparison between the experimental and computed profiles of 10 modes. To avoid nonlinear distortions of the mode profiles, known to occur when the mode amplitude increases too much, the BLS mapping of the mode profiles is performed at microwave power only slightly above threshold. Overall, the measured profiles are in good agreement with the computed ones, taking into account the experimental spatial resolution (approximately 250 nm) and the long duration of these measurements, which are subjected to experimental drifts. Similarly to the analysis performed in Fig. 3, we observe that the mode frequencies obtained by BLS correspond very well to the computed mode frequencies, with a mismatch that remains under 13 MHz for all modes. In particular, we observe well-defined modes up to $n_x = 7$ and $n_y = 3$, which validates the agreement between experiments and simulations for a large number of modes.

III. CONCLUSION

Thanks to the comparison between parametric spectroscopy and mode imaging respectively performed by

MRFM and BLS on the one hand, and micromagnetic simulations on the other hand, we successfully excite, detect and identify a large number (> 40) of SW eigenmodes in a 3-μm YIG disk, where the mode density is large due to the large lateral dimensions. The computed spatial profiles provide a direct way to label those modes, using the numbers of precession nodes in the directions parallel (n_x) and transverse (n_y) to the applied magnetic field. This study opens up the possibility of performing experiments where many parametric modes are simultaneously excited while using the normal mode approach [33,34] to understand and harness the complex dynamics in the modal
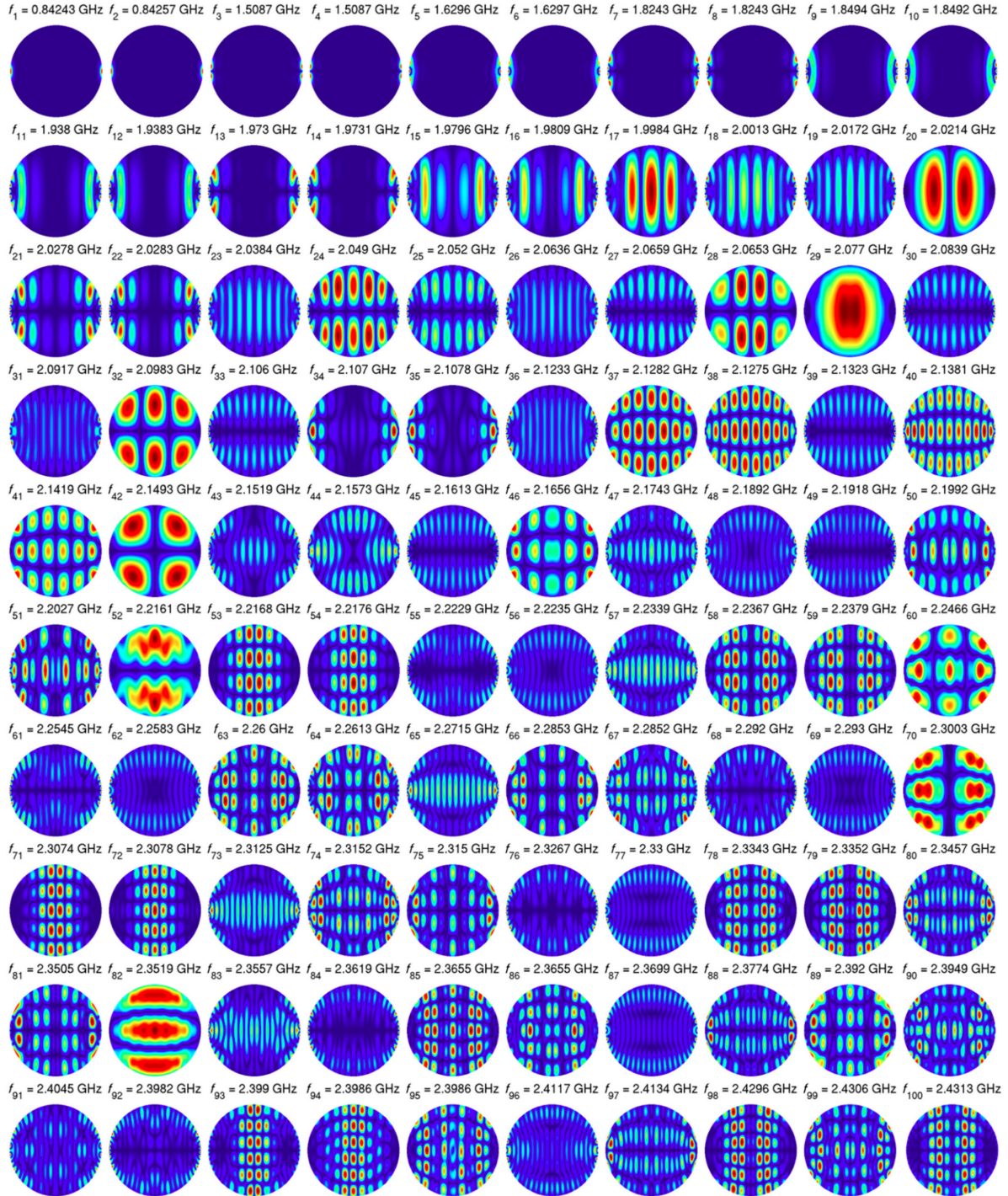

FIG. 6. Computed spatial profiles of the 100 lowest frequency modes of the 3-μm disk. An in-plane field of 27 mT is applied along the horizontal direction. The mode frequencies are indicated on top of the profiles. The color code is the same as in Fig. 4.

space of confined magnetic structures, bringing us a step closer to their applications in unconventional computing.

ACKNOWLEDGMENTS

APPENDIX: 100 LOWEST LYING EIGENMODES

For clarity, only 21 mode profiles are displayed in Fig. 4, those of eigenmodes 11 to 31. Figure 6 presents the 100 lowest frequency modes computed using the micromagnetic eigenmode solver, ordered by their frequency. The eigenfrequencies shown as white vertical ticks in Fig. 3 are those of modes 11 to 69 in Fig. 6.

[1] T. Brächer and P. Pirro, An analog magnon adder for all-magnonic neurons, J. Appl. Phys. **124**, 152119 (2018).

[2] R. Nakane, G. Tanaka, and A. Hirose, Reservoir computing with spin waves excited in a garnet film, IEEE Access **6**, 4462 (2018).

[3] Tyler W. Hughes, Ian A. D. Williamson, Momchil Minkov, and Shanhui Fan, Wave physics as an analog recurrent neural network, Sci. Adv. **5**, 6946 (2019).

[4] Ádám Papp, Wolfgang Porod, and Gyorgy Csaba, Nanoscale neural network using non-linear spin-wave interference, Nat. Commun. **12**, 1 (2021).

[5] Lukas Körber, Christopher Heins, Tobias Hula, Joo-Von Kim, Helmut Schultheiss, Jürgen Fassbender, and Katrin Schultheiss, Pattern recognition with a magnon-scattering reservoir, preprint ArXiv:2211.02328 (2022).

[6] V. V. Naletov, G. de Loubens, G. Albuquerque, S. Borlenghi, V. Cros, G. Faini, J. Grollier, H. Hurdequint, N. Locatelli, B. Pigeau, A. N. Slavin, V. S. Tiberkevich, C. Ulysse, T. Valet, and O. Klein, Identification and selection rules of the spin-wave eigenmodes in a normally magnetized nanopillar, Phys. Rev. B **84**, 224423 (2011).

[7] A. G. Gurevich and G. A. Melkov, *Magnetization Oscillations and Waves* (CRC Press, London, 1996).

[8] R. M. White and M. Sparks, Ferromagnetic relaxation. III. Theory of instabilities, Phys. Rev. **130**, 632 (1963).

[9] H. Kurebayashi, O. Dzyapko, V. E. Demidov, D. Fang, A. J. Ferguson, and S. O. Demokritov, Spin pumping by parametrically excited short-wavelength spin waves, Appl. Phys. Lett. **99**, 162502 (2011).

[10] C. W. Sandweg, Y. Kajiwara, A. V. Chumak, A. A. Serga, V. I. Vasyuchka, M. B. Jungfleisch, E. Saitoh, and B. Hillebrands, Spin Pumping by Parametrically Excited Exchange Magnons, Phys. Rev. Lett. **106**, 216601 (2011).

[11] A. A. Serga, C. W. Sandweg, V. I. Vasyuchka, M. B. Jungfleisch, B. Hillebrands, A. Kreisel, P. Kopietz, and M. P. Kostylev, Brillouin light scattering spectroscopy of parametrically excited dipole-exchange magnons, Phys. Rev. B **86**, 134403 (2012).

[12] C. Hahn, G. de Loubens, M. Viret, O. Klein, V. V. Naletov, and J. Ben Youssef, Detection of Microwave Spin Pumping using the Inverse Spin Hall Effect, Phys. Rev. Lett. **111**, 217204 (2013).

[13] V. Lauer, D. A. Bozhko, T. Brächer, P. Pirro, V. I. Vasyuchka, A. A. Serga, M. B. Jungfleisch, M. Agrawal, Yu. V. Kobljanskyj, G. A. Melkov, C. Dubs, B. Hillebrands, and A. V. Chumak, Spin-transfer torque based damping control of parametrically excited spin waves in a magnetic insulator, Appl. Phys. Lett. **108**, 012402 (2016).

[14] Morteza Mohseni, Martin Kewenig, Roman Verba, Qi Wang, Michael Schneider, Björn Heinz, Felix Kohl, Carsten Dubs, Bert Lägel, Alexander A. Serga, Burkard Hillebrands, Andrii V. Chumak, and Philipp Pirro, Parametric generation of propagating spin waves in ultrathin yttrium iron garnet waveguides, Phys. Status Solidi RRL **14**, 2000011 (2020).

[15] Björn Heinz, Morteza Mohseni, Akira Lentfert, Roman Verba, Michael Schneider, Bert Lägel, Khrystyna Levchenko, Thomas Brächer, Carsten Dubs, Andrii V. Chumak, and Philipp Pirro, Parametric generation of spin waves in nanoscaled magnonic conduits, Phys. Rev. B **105**, 144424 (2022).

[16] Sergei Urazhdin, Vasil Tiberkevich, and Andrei Slavin, Parametric Excitation of a Magnetic Nanocontact by a Microwave Field, Phys. Rev. Lett. **105**, 237204 (2010).

[17] Yu-Jin Chen, Han Kyu Lee, Roman Verba, Jordan A. Katine, Igor Barsukov, Vasil Tiberkevich, John Q. Xiao, Andrei N. Slavin, and Ilya N. Krivorotov, Parametric resonance of magnetization excited by electric field, Nano Lett. **17**, 572 (2017).

[18] Henning Ulrichs, Vladislav E. Demidov, Sergej O. Demokritov, and Sergei Urazhdin, Parametric excitation of eigenmodes in microscopic magnetic dots, Phys. Rev. B **84**, 094401 (2011).

[19] E. R. J. Edwards, H. Ulrichs, V. E. Demidov, S. O. Demokritov, and S. Urazhdin, Parametric excitation of magnetization oscillations controlled by pure spin current, Phys. Rev. B **86**, 134420 (2012).

[20] Feng Guo, L. M. Belova, and R. D. McMichael, Parametric pumping of precession modes in ferromagnetic nanodisks, Phys. Rev. B **89**, 104422 (2014).

[21] T. Brächer, P. Pirro, and B. Hillebrands, Parallel pumping for magnon spintronics: Amplification and manipulation of magnon spin currents on the micron-scale, Phys. Rep. **699**, 1 (2017).

[22] N. Beaulieu, N. Kervarec, N. Thiery, O. Klein, V. Naletov, H. Hurdequint, G. de Loubens, J. Ben Youssef, and N. Vukadinovic, Temperature dependence of magnetic properties of a ultrathin yttrium-iron garnet film grown by liquid phase epitaxy: Effect of a Pt overlayer, IEEE Magn. Lett. **9**, 1 (2018).

[23] Stefan Klingler, A. V. Chumak, Tim Mewes, Behrouz Khodadadi, Claudia Mewes, Carsten Dubs, Oleksii Surzhenko, Burkard Hillebrands, and Andrés Conca, Measurements of the exchange stiffness of YIG films using broadband

ferromagnetic resonance techniques, J. Phys. D: Appl. Phys. **48**, 015001 (2015).

[24] Soraya Sangiao, César Magén, Darius Mofakhami, Grégoire de Loubens, and José Maria De Teresa, Magnetic properties of optimized cobalt nanospheres grown by focused electron beam induced deposition (FEBID) on cantilever tips, Beilstein J. Nanotechnol. **8**, 2106 (2017).

[25] O. Klein, G. de Loubens, V. V. Naletov, F. Boust, T. Guillet, H. Hurdequint, A. Leksikov, A. N. Slavin, V. S. Tiberkevich, and N. Vukadinovic, Ferromagnetic resonance force spectroscopy of individual submicron-size samples, Phys. Rev. B **78**, 144410 (2008).

[26] http://wpage.unina.it/mdaquino/index˙file/MaGICo.html.

[27] Massimiliano d'Aquino, Claudio Serpico, Giovanni Miano, and Carlo Forestiere, A novel formulation for the numerical computation of magnetization modes in complex micromagnetic systems, J. Comput. Phys. **228**, 6130 (2009).

[28] Massimiliano d'Aquino and Riccardo Hertel, Micromagnetic frequency-domain simulation methods for magnonic systems, J. Appl. Phys. **133**, 033902 (2023).

[29] J. Jersch, V. E. Demidov, H. Fuchs, K. Rott, P. Krzysteczko, J. Münchenberger, G. Reiss, and S. O. Demokritov, Mapping of localized spin-wave excitations by near-field Brillouin light scattering, Appl. Phys. Lett. **97**, 152502 (2010).

[30] Feng Guo, L. M. Belova, and R. D. McMichael, Spectroscopy and Imaging of Edge Modes in Permalloy Nanodisks, Phys. Rev. Lett. **110**, 017601 (2013).

[31] H. T. Nembach, Justin M. Shaw, T. J. Silva, W. L. Johnson, S. A. Kim, R. D. McMichael, and P. Kabos, Effects of shape distortions and imperfections on mode frequencies and collective linewidths in nanomagnets, Phys. Rev. B **83**, 094427 (2011).

[32] Vladislav E. Demidov and Sergej O. Demokritov, Magnonic waveguides studied by microfocus Brillouin light scattering, IEEE Trans. Magn. **51**, 1 (2015).

[33] S. Perna, F. Bruckner, C. Serpico, D. Suess, and M. d'Aquino, Computational micromagnetics based on normal modes: Bridging the gap between macrospin and full spatial discretization, J. Magn. Magn. Mater. **546**, 168683 (2022).

[34] S. Perna, F. Bruckner, C. Serpico, D. Suess, and M. d'Aquino, Normal modes description of nonlinear ferromagnetic resonance for magnetic nanodots, AIP Adv. **12**, 035244 (2022).